

# DUAL CROSS-ATTENTION SIAMESE TRANSFORMER FOR RECTAL TUMOR REGROWTH ASSESSMENT IN WATCH-AND-WAIT ENDOSCOPY

Jorge Tapias Gomez<sup>1</sup> Despoina Kanata<sup>2</sup> Aneesh Rangnekar<sup>1</sup> Christina Lee<sup>2</sup>  
Julio Garcia-Aguilar<sup>2</sup> Joshua Jesse Smith<sup>2</sup> Harini Veeraraghavan<sup>1</sup>

<sup>1</sup> Department of Medical Physics, Memorial Sloan Kettering Cancer Center, USA

<sup>2</sup> Department of Surgery, Colorectal Service, Memorial Sloan Kettering Cancer Center, USA

Increasing evidence supports watch-and-wait (WW) surveillance for patients with rectal cancer who show clinical complete response (cCR) at restaging following total neoadjuvant treatment (TNT). However, objectively accurate methods to early detect local regrowth (LR) from follow-up endoscopy images during WW are essential to manage care and prevent distant metastases. Hence, we developed a Siamese Swin Transformer with Dual Cross-Attention (SSDCA) to combine longitudinal endoscopic images at restaging and follow-up and distinguish cCR from LR. SSDCA leverages pretrained Swin transformers to extract domain agnostic features and enhance robustness to imaging variations. Dual cross attention is implemented to emphasize features from the two scans without requiring any spatial alignment of images to predict response. SSDCA as well as Swin-based baselines were trained using image pairs from 135 patients and evaluated on a held-out set of image pairs from 62 patients. SSDCA produced the best balanced accuracy ( $81.76\% \pm 0.04$ ), sensitivity ( $90.07\% \pm 0.08$ ), and specificity ( $72.86\% \pm 0.05$ ). Robustness analysis showed stable performance irrespective of artifacts including blood, stool, telangiectasia, and poor image quality. UMAP clustering of extracted features showed maximal inter-cluster separation ( $1.45 \pm 0.18$ ) and minimal intra-cluster dispersion ( $1.07 \pm 0.19$ ) with SSDCA, confirming discriminative representation learning.

## 1. INTRODUCTION

The Organ Preservation in Rectal Adenocarcinoma (OPRA) clinical trial (NCT02008656) showed that 47% of patients with rectal adenocarcinoma treated with total neoadjuvant therapy (TNT) followed by a watch-and-wait (WW) surveillance avoid surgery and achieve sustained clinical response without reducing their chance of cure [1]. Subjective clinical assessment is only 65% accurate, and suffers from large inter-rater variation [2], necessitating objectively accurate methods to distinguish sustained clinical response (cCR) from local regrowth (LR) for optimal patient management.

Although deep learning (DL) methods have shown capability to detect tumor response at restaging (8 to 12 weeks

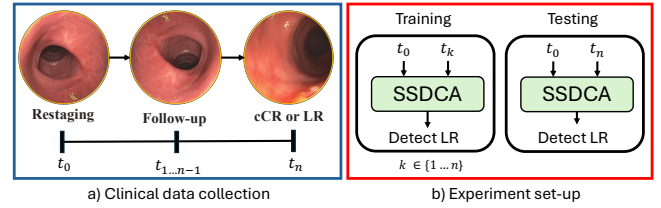


**Fig. 1.** (a) Endoscopic images acquired every three months during watch-and-wait, producing a longitudinal sequence from  $t_0$  to  $t_n$ . (b) Training and testing setup in which image pairs from different timepoints are combined and provided as input into the Siamese Swin Dual Cross-Attention (SSDCA) model.

after TNT) [3, 4, 5], such methods are less accurate when applied to detect regrowing tumors that exhibit large variations in appearance, shape, and confounding factors such as blood [4]. However, an important feature in the management of patients on WW is the acquisition of multiple follow-up images until LR is detected or patients show sustained cCR for 3 years following TNT completion/restaging (Figure 1). Hence, we hypothesized that extracting the change in image features from restaging to follow-up would provide more accurate prediction of LR.

Longitudinal endoscopic image analysis involves challenges including lack of spatial registration between images acquired at different times, variable number of follow ups due to differences in tumor regrowth patterns, and presence of varied artifacts such as blood, stool, telangiectasia, and scope that confound accurate detection [6]. Our contribution addresses these challenges by developing: (a) a Siamese architecture combining temporal features from restaging and follow-up images through bi-directional cross attention, obviating need for spatial alignment, (b) pretrained Swin encoders to enhance robustness to underlying image variations and we performed to study the impact of commonly occurring artifacts in endoscopic images, and (c) preliminary interpretability study to assess spatial similarity of the attentions from the two time points for classification.

## 2. RELATED WORKS

Multiple prior works have addressed the problem of predicting tumor treatment response by combining pairs of images either using radiomic [7] or DL methods involving radiographic CT and MR images [8, 9, 10, 11, 12], demonstrating the benefit of combining additional time point in improving prediction accuracy. Methods to fuse information from temporal images vary, ranging from simple feature differencing [7], image or features concatenation [8] to cross-attention formulations [10, 9]. Long short term memory networks have also been used to model the temporal dynamics of feature changes between subsequent images acquired at fixed imaging intervals such as every week during radiation treatment [13]. However, aforementioned approaches require voxel-wise spatial correspondence between images achieved either through registration [8] or by focusing on region of interest centered on the detected tumors [9] to extract meaningful information. Such spatial registration is harder to achieve for endoscopic images captured from potentially different view points and highly variable follow up times. Our approach addresses these gaps by using a dual cross attention formulation implemented by adapting Siamese neural network (SNN) [14] representation of pretrained Swin Transformer encoder. Importantly, computed cross-attentions are then combined using residual connections with the corresponding features to emphasize relevant features to reliably detect LR.

## 3. METHODS

### 3.1. Datasets

One hundred ninety seven patients with LARC treated with induction or consolidation total neoadjuvant therapy (TNT) and selected for WW surveillance at restaging (8 to 12 weeks after completing TNT) were analyzed to classify LR vs. cCR using pairs of endoscopic images at restaging and a follow-up. A total of 2,278 images (LR = 768, cCR = 1,510) were available for use. Model training was performed using 7,392 image pairs (restaging and intermediate follow-up as well as temporally ordered pairs of follow-ups) from 135 patients. Testing was performed on a held-out set of 368 image pairs (restaging and last follow up) from 62 patients as gold standard ground truth was only available after last follow up, when patients go for surgery or are determined to have sustained cCR. As a result, labels for training used the ground truth from final follow-up, even if LR or evidence of cCR may not be apparent to surgeons from the intermediate follow-ups, presenting a more challenging training with imperfect labels scenario.

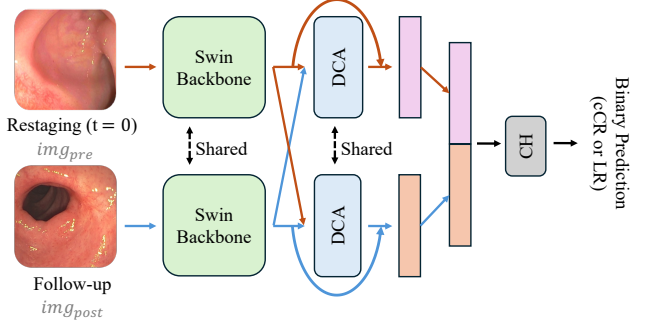


Fig. 2. Architecture overview of the model.

### 3.2. Network architecture

Figure 2 depicts an overview of our approach. As shown a Siamese neural network (SNN) with a hierarchical shifted window (Swin) Transformer encoder [15] is used to extract features from images taken at two time points. In order to reduce the impact of spatial misalignments and reduce the computational demands, the features from stage #4 are combined through the dual cross-attention (DCA) module. DCA emphasizes features across the time points, which then are used as residual inputs to the corresponding features, concatenated, and then combined through a classification head (CH) to generate classification as cCR versus LR.

### 3.3. Dual Cross Attention (DCA)

The DCA module focuses on relevant features in one image by attending to features occurring in similar spatial locations in the other image by learned cross attention [16]. In this way, the need for spatial alignment of images prior to their use for combined prediction is less important.

A pair of longitudinal images  $x_{pre}, x_{post}$  are tokenized and processed by a shared Swin encoder  $f_{\theta}$ . The stage #4 features from the two images  $F_{pre} = f_{\theta}^{(4)}(x_{pre})$  and  $F_{post} = f_{\theta}^{(4)}(x_{post})$  with shape  $H/32 \times W/32 \times C$ , where  $H$  and  $W$  correspond to the pixel resolution, and  $C$  to the number of channels are extracted. A Swin encoder was used to alleviate the need to embed absolute positional information as is required in a vision transformer (ViT). As such the relative spatial encoding focuses on extracting the local relationships and local spatial bias, which complements the cross attention extracted by the DCA to extract correspondences between the features in the two images.

Concretely, cross attention is performed by flattening the spatial dimensions of  $F_{pre}$  and  $F_{post}$  and reshaping into matrices of size  $(H/32 \cdot W/32) \times C$ . Cross attention operation is performed in both directions by using features from each image as queries ( $q_{pre} = F_{pre}W_q$  and  $q_{post} = F_{post}W_q$ ) and the other as key ( $k_{pre} = F_{pre}W_k$ ,  $k_{post} = F_{post}W_k$ ), value pairs ( $v_{pre} = F_{pre}W_v$  and  $v_{post} = F_{post}W_v$ ) and vice

versa, which ensures that the fused representation appropriately emphasizes spatially aligned features in both timepoints.  $W_q, W_k, W_v \in \mathbb{R}^{C \times 3C_h}$  are the learned projection matrices.

$$\text{CA}(F_{pre}) = \text{softmax}\left(q_{pre}k_{post}^\top / \sqrt{D_h}\right) v_{post} \quad (1)$$

$$\text{CA}(F_{post}) = \text{softmax}\left(q_{post}k_{pre}^\top / \sqrt{D_h}\right) v_{pre} \quad (2)$$

Residual connections and layer normalization (LN) are then applied:

$$H_{pre} = \text{LN}(F_{pre} + \text{CA}(F_{pre})) \quad (3)$$

$$H_{post} = \text{LN}(F_{post} + \text{CA}(F_{post})) \quad (4)$$

Finally, global average pooling (GAP) is applied to  $H_{pre}$  and  $H_{post}$ , and the pooled features are concatenated and passed through the classification head:

$$p = \sigma\left(\text{CH}(\text{concat}(\text{GAP}(H_{pre}), \text{GAP}(H_{post})))\right) \quad (5)$$

where  $\sigma$  denotes the sigmoid output probability. This dual formulation yields a registration-free, correspondence-aware representation of longitudinal changes without requiring explicit registration.

### 3.4. Implementation Details

We used the Swin-Small variant with a patch size of  $4 \times 4$  and window size of  $7 \times 7$  for  $224 \times 224$  inputs, initialized with ImageNet-pretrained weights [17]. All layers were fine-tuned. The classification head consisted of a linear layer, ReLU, dropout, and a final linear layer, producing logits corresponding to the tumor regrowth probability (class = 1).

In addition, Swin-based variants consisting of **Swin Small Single Image (Swin-S SI)**, which serves as a non-Siamese baseline [3], and a simple feature concatenation based approach called **SSFC**, which performs feature concatenation at Stage 4 were trained and tested with identical data as SSDCA.

All models were fine-tuned using Adam (learning rate  $2 \times 10^{-4}$ ) with a linear scheduler and 10-epoch warmup, and trained for 30 epochs with cross-entropy loss and a batch size of 8. Data augmentation included random  $90^\circ$  rotations, horizontal flips, and vertical flips to address the limited size of colonoscopy datasets [18]. Balanced sampling was applied to mitigate class imbalance. To ensure robust performance in the low-data regime, we performed stratified 5-fold cross-validation. For each fold, the model with the best validation accuracy was selected, and reported results correspond to the mean and standard deviation across folds. All experiments were conducted in PyTorch 1.13.1 on NVIDIA GPUs.

### 3.5. Metrics

For patients with multiple images acquired on the same day, predictions were aggregated using a top- $k$  strategy ( $k=3$ ).

**Table 1.** Testing data accuracy for analyzed models averaging the predictions from the 5-fold cross-validated models.

Model	Balanced Accuracy	Sensitivity	Specificity
Swin-S SI	$76.24 \pm 0.02$	$65.32 \pm 0.09$	$87.14 \pm 0.07$
SSFC	$81.13 \pm 0.06$	$84.00 \pm 0.13$	$78.57 \pm 0.12$
SSDCA	$81.76 \pm 0.05$	$90.07 \pm 0.08$	$72.86 \pm 0.05$

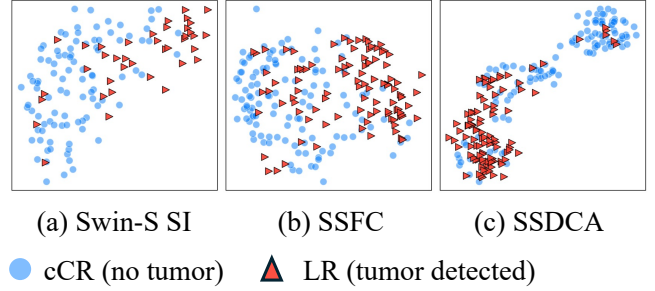


**Fig. 3.** UMAP visualization of feature embeddings from the testing set. Each point represents an image combination (or a single image for Swin-S SI), color-coded by final clinical outcome. LR = local regrowth, cCR = complete clinical response.

Model accuracy was evaluated with respect to the "gold standard" ground truth obtained only after the last followup, or the longitudinal endpoint. Balanced accuracy, specificity, and sensitivity were computed. Significance tests to measure model differences were computed using paired t-tests with a 95% confidence interval. Robustness to common imaging artifacts such as telangiectasia (TLG), blood, stool, and poor quality (PQ) that includes specular reflections, image over or under-saturation, occlusions from presence of scope was analyzed by computing specificity and sensitivity under these conditions.

## 4. RESULTS

### 4.1. SSDCA more accurately predicts LR

As shown in Table 1, SSDCA was the most accurate followed by SSFC. As shown, SSDCA had higher sensitivity than SSFC but lower specificity than the latter method. On the other hand, using only single image prediction was the least accurate, with a much lower sensitivity ( $p = 0.0029$  95% CI: [0.1454, 0.3613]) and sensitivity ( $p = 0.0088$ ) than SSDCA. **CHECK THIS IN CASE WE CAN GET BETTER SIGNICANCE**

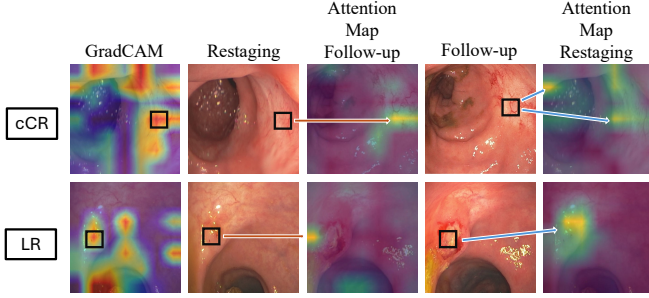


**Fig. 4.** GradCAM and attention maps for two representative test cases produced using SSDCA shows good correspondence of relevant spatial features between the images.

#### 4.2. SSDCA features are better separated indicating better discrimination for classification

Fig. 3 shows the UMAP projections of the features computed from the test cases using the different models. As shown, SSDCA produced the best separation of patients by outcomes, achieving the highest inter-cluster distance ( $1.45 \pm 0.18$ ) and lowest intra-cluster spread ( $1.07 \pm 0.19$ ). In contrast, both Swin-S SI and SSFC exhibited reduced separation ( $1.18 \pm 0.21$  and  $1.38 \pm 0.19$ , respectively) and large spatial spread of the clusters ( $1.10 \pm 0.06$  and  $1.22 \pm 0.09$ ). On the other hand, SSDCA resulted in tighter margins ( $\approx +0.25$  inter,  $-0.15$  intra) confirming why better discrimination of patient outcomes resulted from this method.

#### 4.3. Attention map correspondences between temporal image pairs with SSDCA

Fig. 4 visualizes the spatial correspondences between the attended features in the restaging and the follow-up images for two representative test cases. GradCAM is used to extract the relevant regions used for prediction using the restaging image. A sample selected region with high attention shows correspondingly high activation in the attention map from the restaging image, despite lack of any spatial alignment between the two images. Finally, the high attention region from follow-up image was used to compared to the attended region in the restaging, which shows strong correspondence for the LR case (second row) and high activation in the corresponding as well as additional regions for the cCR case. The selected cases contained variations also due to presence of blood and specular reflection from mucosa.

#### 4.4. Robustness analysis

Fig. 5 shows the output probability distributions of the SSDCA model under different imaging variations (Blood, Stool, TLG, and PQ). SSDCA performs well under blood, correctly identifying most tumor cases, which may suggest that visible bleeding can indicate a regrowth and thus make detection

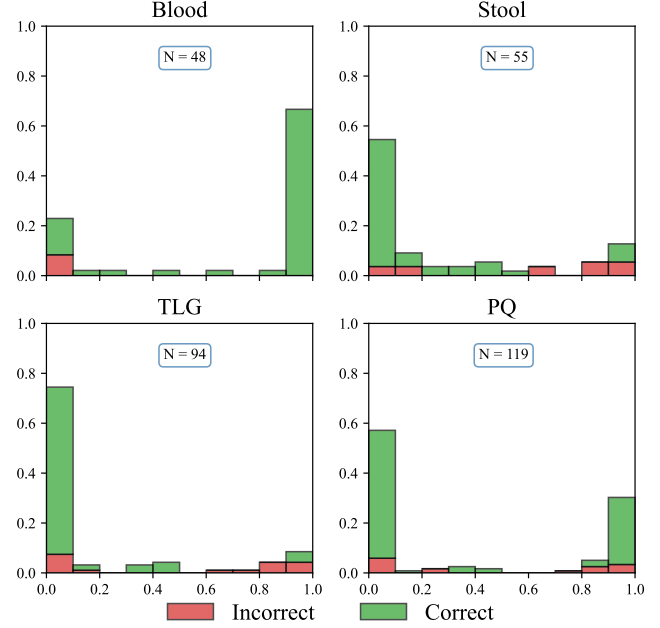


**Fig. 5.** SSDCA output probability distributions under different imaging variations (blood, stool, TLG, and PQ). Green represents the correctly predicted sample, and red the incorrectly predicted samples.

easier. In contrast, the model has difficulty detecting tumors when exposed to stool and TLG. This is likely because stool may obscure visual cues, and TLG is a known marker of clinical complete response [6]. Under PQ, the model struggles for both tumor and no-tumor cases, which is expected as low-quality or blurry images provide less reliable information for overall correct classification.

#### 4.5. Ablation analysis: Impact of stage used for feature fusion

Impact of computing DCA with the different stages of the swin backbone (Stage 1, Stage 2, Stage 3, and Stage 4) was evaluated. Late fusion at **Stage 4** achieved the highest balanced accuracy (82%) and sensitivity (78%), while earlier fusion layers provided no benefit. Thus, deeper fusion—where features encode semantically richer spatial cues—yields the most discriminative cross-pair representations.

## 5. DISCUSSION AND CONCLUSION

We developed a longitudinal analysis framework to predict tumor regrowth from endoscopic images of rectal cancer patients. Our findings show that combining pairs of images with dual cross attention leads to more accurate performance compared to single time-point analysis. SSDCA balanced accuracy of 82% is comparable to surgeons' accuracy ranging

between 74% to 83% to detect LR [19]. Our analysis also showed that DCA extracted spatially similar features despite lack of spatial alignment between images to inform prediction. Finally, SSDCA was reasonably robust to common endoscopic artifacts, suggesting that it is a reasonable approach for endoscopic image based prediction of treatment response.

## 6. COMPLIANCE WITH ETHICAL STANDARDS

This retrospective research study was conducted in line with the principles of the Declaration of Helsinki. Approval was granted by the Ethics Committee of Memorial Sloan Kettering Cancer Center.

## 7. ACKNOWLEDGEMENTS

This research was supported by Department of Surgery at Memorial Sloan Kettering. We thank Maria Widmar, Iris H Wei, Emmanouil P Pappou, Garrett M Nash, Martin R Weiser, and Philip B Paty, along with Hannah Thompson, Hannah Williams, Joshua Jesse Smith and Julio Garcia-Aguilar, for their assistance in collecting endoscopic images.

## 8. REFERENCES

- [1] Julio Garcia-Aguilar, Sujata Patil, Marc J. Gollub, Jin K. Kim, Jonathan B. Yuval, Hannah M. Thompson, Floris S. Verheij, Dana M. Omer, Meghan Lee, Richard F. Dunne, Jorge Marcet, Peter Cataldo, Blase Polite, Daniel O. Herzig, David Liska, Samuel Oommen, Charles M. Friel, Charles Terner, Andrew L. Coveler, Steven Hunt, Anita Gregory, Madhulika G. Varma, Brian L. Bello, Joseph C. Carmichael, John Krauss, Ana Gleisner, Philip B. Paty, Martin R. Weiser, Garrett M. Nash, Emmanouil Pappou, José G. Guillem, Larissa Temple, Iris H. Wei, Maria Widmar, Sabrina Lin, Neil H. Segal, Andrea Cercek, Rona Yaeger, J. Joshua Smith, Karyn A. Goodman, Abraham J. Wu, and Leonard B. Saltz, “Organ preservation in patients with rectal adenocarcinoma treated with total neoadjuvant therapy,” *Journal of Clinical Oncology*, vol. 40, no. 23, pp. 2546–2556, 2022, PMID: 35483010.
- [2] Seth I. Felder, Sujata Patil, Erin Kennedy, and Julio Garcia-Aguilar, “Endoscopic feature and response reproducibility in tumor assessment after neoadjuvant therapy for rectal adenocarcinoma,” *Annals of Surgical Oncology*, vol. 28, no. 9, pp. 5205–5223, 2021.
- [3] Jorge Tapias Gomez, Aneesh Rangnekar, Hannah Williams, Hannah M. Thompson, Julio Garcia-Aguilar, Joshua Jesse Smith, and Harini Veeraraghavan, “Swin transformers are robust to distribution and concept drift in endoscopy-based longitudinal rectal cancer assessment,” in *Medical Imaging 2025: Image Processing*, Olivier Colliot and Jhimli Mitra, Eds. International Society for Optics and Photonics, 2025, vol. 13406, p. 134061N, SPIE.
- [4] Hannah Williams, Hannah M. Thompson, Christina Lee, Aneesh Rangnekar, Jorge T. Gomez, Maria Widmar, Iris H. Wei, Emmanouil P. Pappou, Garrett M. Nash, Martin R. Weiser, Philip B. Paty, J. Joshua Smith, Harini Veeraraghavan, and Julio Garcia-Aguilar, “Assessing endoscopic response in locally advanced rectal cancer treated with total neoadjuvant therapy: Development and validation of a highly accurate convolutional neural network,” *Annals of Surgical Oncology*, vol. 31, no. 10, pp. 6443–6451, Oct 2024.
- [5] Hester Haak, Xinpei Gao, Monique Maas, Selam Waktoła, Sean Benson, Regina Beets-Tan, Geerard Beets, Monique Leerdam, and Jarno Melenhorst, “The use of deep learning on endoscopic images to assess the response of rectal cancer after chemoradiation,” *Surgical Endoscopy*, vol. 36, pp. 1–9, 10 2021.
- [6] H. Thompson, J.K. Kim, R.M. Jimenez-Rodriguez, J. Garcia-Aguilar, and H. Veeraraghavan, “Deep learning-based model for identifying tumors in endoscopic images from patients with locally advanced rectal cancer treated with total neoadjuvant therapy,” *Dis Colon Rectum*, vol. 66, no. 3, pp. 383–391, 2023.
- [7] Elizabeth J. Sutton, Natsuko Onishi, Duc A. Fehr, Brittany Z. Dashevsky, Meredith Sadinski, Katja Pinker, Danny F. Martinez, Edi Brogi, Lior Braunstein, Pedram Razavi, Mahmoud El-Tamer, Virgilio Sacchini, Joseph O. Deasy, Elizabeth A. Morris, and Harini Veeraraghavan, “A machine learning model that classifies breast cancer pathologic complete response on mri post-neoadjuvant chemotherapy,” *Breast Cancer Research*, vol. 22, no. 1, pp. 57, 2020.
- [8] Cheng Jin, Heng Yu, Jia Ke, Peirong Ding, Yongju Yi, Xiaofeng Jiang, Xin Duan, Jinghua Tang, Daniel T. Chang, Xiaojian Wu, Feng Gao, and Ruijiang Li, “Predicting treatment response from longitudinal images using multi-task deep learning,” *Nature Communications*, vol. 12, no. 1, pp. 1851, 2021.
- [9] Yuchen Sun, Kunwei Li, Duanduan Chen, Yi Hu, and Shuaitong Zhang, “Lomia-t: A transformer-based longitudinal medical image analysis framework for predicting treatment response of esophageal cancer,” in *Medical Image Computing and Computer Assisted Intervention – MICCAI 2024*, Marius George Linguraru, Qi Dou, Aasa Feragen, Stamatia Giannarou, Ben Glocker, Karim Lekadir, and Julia A. Schnabel, Eds., Cham, 2024, pp. 426–436, Springer Nature Switzerland.



- [10] Hailin Yue, Jin Liu, Junjian Li, Hulin Kuang, Jinyi Lang, Jianhong Cheng, Lin Peng, Yongtao Han, Harrison Bai, Yuping Wang, Qifeng Wang, and Jianxin Wang, “Mldrl: Multi-loss disentangled representation learning for predicting esophageal cancer response to neoadjuvant chemoradiotherapy using longitudinal ct images,” *Medical Image Analysis*, vol. 79, pp. 102423, 2022.
- [11] Matthew Li, Ken Chang, Ben Bearce, Connie Chang, Ambrose Huang, John Campbell, James Brown, Praveer Singh, Katharina Hoebel, Deniz Erdogmus, Stratis Ioannidis, William Palmer, Michael Chiang, and Jayashree Kalpathy-Cramer, “Siamese neural networks for continuous disease severity evaluation and change detection in medical imaging,” *npj Digital Medicine*, vol. 3, 12 2020.
- [12] Heejong Kim, Batuhan K. Karaman, Qingyu Zhao, Alan Q. Wang, Mert R. Sabuncu, and the Alzheimer’s Disease Neuroimaging Initiative, “Learning-based inference of longitudinal image changes: Applications in embryo development, wound healing, and aging brain,” *Proceedings of the National Academy of Sciences*, vol. 122, no. 8, pp. e2411492122, 2025.
- [13] Yiwen Xu, Ahmed Hosny, Roman Zeleznik, Chintan Parmar, Thibaud Coroller, Idalid Franco, Raymond H. Mak, and Hugo J. W. L. Aerts, “Deep learning predicts lung cancer treatment response from serial medical imaging,” *Clinical Cancer Research*, vol. 25, no. 11, pp. 3266–3275, 2019.
- [14] Jane Bromley, Isabelle Guyon, Yann LeCun, Eduard Säckinger, and Roopak Shah, “Signature verification using a ”siamese” time delay neural network,” in *Proceedings of the 7th International Conference on Neural Information Processing Systems*, San Francisco, CA, USA, 1993, NIPS’93, p. 737–744, Morgan Kaufmann Publishers Inc.
- [15] Ze Liu, Yutong Lin, Yue Cao, Han Hu, Yixuan Wei, Zheng Zhang, Stephen Lin, and Baining Guo, “Swin transformer: Hierarchical vision transformer using shifted windows,” 2021.
- [16] Wen Lu, Lu Wei, and Minh Nguyen, “Bitemporal attention transformer for building change detection and building damage assessment,” *IEEE Journal of Selected Topics in Applied Earth Observations and Remote Sensing*, vol. 17, pp. 4917–4935, 2024.
- [17] Jia Deng, Wei Dong, Richard Socher, Li-Jia Li, Kai Li, and Li Fei-Fei, “Imagenet: A large-scale hierarchical image database,” in *2009 IEEE Conference on Computer Vision and Pattern Recognition*, 2009, pp. 248–255.
- [18] Sanat Ramesh, Vinkle Srivastav, Deepak Alapatt, Tong Yu, Aditya Murali, Luca Sestini, Chinedu Innocent Nwoye, Idris Hamoud, Saurav Sharma, Antoine Fleurentin, Georgios Exarchakis, Alexandros Karagyris, and Nicolas Padoy, “Dissecting self-supervised learning methods for surgical computer vision,” 2023.
- [19] Hannah Williams, Hannah M Thompson, Sabrina T Lin, Floris S Verheij, Dana M Omer, Li-Xuan Qin, Julio Garcia-Aguilar, OPRA Consortium, et al., “Endoscopic predictors of residual tumor after total neoadjuvant therapy: a post hoc analysis from the organ preservation in rectal adenocarcinoma trial,” *Diseases of the Colon & Rectum*, vol. 67, no. 3, pp. 369–376, 2024.